3*nj* Morphogenesis and Semiclassical Disentangling[†]

Roger W. Anderson

Department of Chemistry, University of California, Santa Cruz, California 95064

Vincenzo Aquilanti

Dipartimento di Chimica, Università degli Studi di Perugia, via Elce di Sotto 8, 06126 Perugia, Italy

Annalisa Marzuoli*

Dipartimento di Fisica Nucleare e Teorica, Università degli Studi di Pavia and INFN, Sezione di Pavia, via A. Bassi 6, 27100 Pavia, Italy

Received: June 3, 2009; Revised Manuscript Received: September 2, 2009

Recoupling coefficients (3*nj* symbols) are unitary transformations between binary coupled eigenstates of $N = (n + 1)$ mutually commuting $SU(2)$ angular momentum operators. They have been used in a variety of applications in spectroscopy, quantum chemistry and nuclear physics and quite recently also in quantum gravity and quantum computing. These coefficients, naturally associated to cubic Yutsis graphs, share a number of intriguing combinatorial, algebraic, and analytical features that make them fashinating objects to be studied on their own. In this paper we develop a bottom-up, systematic procedure for the generation of 3*nj* from $3(n - 1)j$ diagrams by resorting to diagrammatical and algebraic methods. We provide also a novel approach to the problem of classifying various regimes of semiclassical expansions of 3*nj* coefficients (asymptotic disentangling of 3*nj* diagrams) for $n \geq 3$ by means of combinatorial, analytical and numerical tools.

Introduction

In the quantum theory of angular momentum—mathematically encoded in $SU(2)$ representation theory—the study of (re)coupling of pure eigenstates of several, mutually commuting angular momentum operators $\mathbf{J}_1$, $\mathbf{J}_2$, ..., $\mathbf{J}_N$ is considered an advanced topic, and as such it is not widely known. As pointed out in the classic ref 1 (topic 12):

We shall deal with what is appropriately called the theory of binary coupling of angular momenta, since it is a theory in which one couples angular momenta sequentially, in pairs. ... Accordingly, the theory deals with the relationships between different coupling schemes—that is between distinct sequences of pairwise couplings. This is the content of recoupling theory. The subject is a difficult one and the literature is extensive. Several monographs [e.g., refs 2−5[6]*] deal with techniques for implementing "graphical" methods (...).*

This paper is much in the spirit of the program stated soon after that, namely

Our goal is to relate coupling methods to standard results from graph theory. The subject divides quite naturally into three parts:

(A) (the classification of coupling schemes)

(B) the elementary operations underlying the structure of transformation (recoupling) coefficients, or 3nj symbols

(C) the classification of recoupling coefficients and its relationship to the theory of cubic graphs

We are going to deal first with (B) and (C) above by formalizing an effective, step-by-step method to build up 3*nj* coefficients of types I and II from $3(n - 1)j$'s of the same type (note that, by convention, the integer n is related to the N angular momenta introduced above by $(n + 1) = N$).

Our second goal is to take advantage of such a recursive construction in the search for a novel unifying scheme for addressing semiclassical limits (asymptotic expansions) of the 3*nj* themselves. This task calls into play different techniques, both analytical and numerical and is very important in view of practical applications (that have been discussed extensively elsewhere).

1. Recursion Method for 3*nj* Coefficients: General Description

The diagram of any $SU(2)$ 3*nj* coefficient is a cubic (regular trivalent) graph on $3n$ lines and $2n$ nodes, named a Yutsis graph from the first author of ref 2. The three edges stemming from each node are associated with a triad of angular momentum quantum numbers satisfying triangle inequalities, i.e., to a Wigner 3*j* coefficient. This property of diagrams reflects the fact that any 3*nj* can be always written as a sum over all magnetic quantum numbers of the product of $2n$ (suitably chosen) 3*j* coefficients (see e.g., ref 5 Chapter 9).

The recursion method for the generation of (all) 3*nj* diagrams with increasing n may be summarized as in ref 2 p 65

(Recursion rule) *The diagrams of the 3nj coefficients are obtained from the diagrams of the 3(n − 1)j by inserting two additional nodes on any two lines of the diagram of the 3(n − 1)j coefficients and joining them together.*

There are some caveats underlying this combinatorial construction: it must generate diagrams that are not separable on

[†] Part of the "Vincenzo Aquilanti Festschrift".

* Corresponding author. E-mail: annalisa.marzuoli@pv.infn.it.

10.1021/jp905212a
Published on Web 10/13/2009

fewer than four lines and this is achieved by requiring that the initial 3*nj* diagram is separable on no fewer than three lines (examples are provided below); moreover, isomorphic configurations should be recognized and ruled out.[7]

Algebraic expressions ("recurrence formulas") that encode the above combinatorial prescription on diagrams are provided for the 3*nj* coefficients of the first (I) and second (II) type in ref 3 ((24.8) p 81 and (A.6.14) p 143), respectively and read

$$(-1)^{\Phi}\sum_x (2x+1)\begin{Bmatrix} j_1 & \cdots & j_{n-1} \\ & l_1 \ \cdots \ l_{n-2} & \\ k_1 & \cdots & k_{n-1} \end{Bmatrix} \begin{Bmatrix} j_1 & k_{n-1} & x \\ l_{n-1} & l_2 & k_n \end{Bmatrix}\begin{Bmatrix} k_1 & j_{n-1} & x \\ l_{n-1} & l_n & j_n \end{Bmatrix} = \begin{Bmatrix} j_1 & \cdots & j_n \\ & l_1 \ \cdots & \\ k_1 & \cdots & k_n \end{Bmatrix} \quad (1)$$

where $\Phi = j_1 - k_1 - j_{n-1} + k_{n-1}$, and

$$(-1)^{\Psi}\sum_x (2x+1)\begin{bmatrix} j_1 & \cdots & j_{n-1} \\ & l_1 \ \cdots \ l_{n-2} & \\ k_1 & \cdots & k_{n-1} \end{bmatrix} \begin{Bmatrix} k_1 & k_{n-1} & x \\ l_{n-1} & l_n & k_n \end{Bmatrix}\begin{Bmatrix} j_1 & j_{n-1} & x \\ l_{n-1} & l_n & j_n \end{Bmatrix} = \begin{bmatrix} j_1 & \cdots & j_n \\ & l_1 \ \cdots & \\ k_1 & \cdots & k_n \end{bmatrix} \quad (2)$$

where $\Psi = j_1 - k_1 + j_{n-1} - k_{n-1}$. Here the angular momenta variables $\{k_1, ..., l_1, ..., j_1, ...\}$ run over either $\{0, 1, 2, ...\}$ or $\{1/2, 3/2, ...\}$ and satisfy suitable triangle inequalities. The summation variable x is also constrained by triangle relations.

The roles played by the expressions (1) and (2) are multiple and interconnected:

(i) At face value they provide a straightforward decomposition of a 3*nj* coefficient into a single sum involving one $3(n-1)j$ of the same type and exacly two Wigner 6*j* symbols.
(Note, however, that these decompositions are not the basic ones for computational purposes, since it is well-known that both types of coefficients may be expressed as single sums of products of *n* 6*j* symbols; cf. eqs 1 and 2, p 361 in ref 5.)

(ii) From the structural point of view, they encode also generalizations of the basic Biedenharn−Elliott identity (see the case of 9*j* generation in section 2 where these two aspects of (1) and (2) are worked out explicitly).

(iii) Taking advantage of symmetries of (any kind of) 3*nj* coefficients, one can equate two different decompositions related by a symmetry of a same 3*nj* to get relations for the associated $3(n-1)j$ coefficients. For instance the relations derived from (1) have the following general structure (dropping phases and omitting all the arguments not relevant in the present discussion)

$$\sum_x \begin{Bmatrix} \bullet & \bullet & x \\ \bullet & \lambda & \bullet \end{Bmatrix}\begin{Bmatrix} \bullet & \cdots & \\ & \bullet & \\ \bullet & \cdots & \end{Bmatrix}\begin{Bmatrix} \cdots & x \\ \bullet & \bullet \\ \cdots & \end{Bmatrix}\begin{Bmatrix} \bullet & \bullet & x \\ \bullet & \lambda & \bullet \end{Bmatrix} = \sum_y \begin{Bmatrix} \bullet & \bullet & y \\ \bullet & \lambda & \bullet \end{Bmatrix}\begin{Bmatrix} \bullet & \cdots & \\ & \bullet & \\ \bullet & \cdots & \end{Bmatrix}\begin{Bmatrix} \cdots & y \\ \bullet & \bullet \\ \cdots & \end{Bmatrix}\begin{Bmatrix} \bullet & \bullet & y \\ \bullet & \lambda & \bullet \end{Bmatrix} \quad (3)$$

Specifying $\lambda = 1/2, 1, 3/2, 2$, etc. and using explicit forms of the resulting 6*j* symbols, various recursion relations may be obtained (note that the sums on both sides of (3) reduce to a same number of terms, e.g., for $\lambda = 1/2$ one would get $x, y = 0, 1$). The case of the 9*j* symbol and associated 5-term recursion relation will be worked out in section 2.2.
The case of the 6*j* symbol is quite subtle since the well-known three-term recursion relation in one variable—used in refs 9, 10, and 1 (topic 9) as a second-order difference equation to be analyzed within the WKB framework—actually derives directly from (2), which is nothing but the standard Biedenharn−Elliott identity (see also (5) in the next section). This remark has to do with a deep property of hypergeometric polynomials in the Askey scheme:[11] the defining difference or differential equation and the recursion relation are usually "dual" to each other but the 6*j* happens to be "self-dual" so that the two viewpoints can be used equivalently.

(iv) Decompositions like those given in (1) and (2), as well as associated recurrence relations, can be also employed in the opposite direction, namely to show how a 3*nj* symbol falls back into a $3(n-1)j$ when one of its entry is set to zero. This well-known feature[5] will be used in remark (i) at the end of section 2.2.

The bottom-up recursion method, fully developed in this paper by resorting to both diagrammatical and algebraic tools,[2,3,5] not only represents a systematic procedure for the generation of 3*nj*'s from $3(n-1)j$ diagrams (section 3) but also will provide a novel approach to the classification of the (various regimes of) asymptotic disentangling of the coefficients themselves (section 4), improving and extending previous results for the 9*j* found in ref 12.

To make the reader familiar with diagrammatic and algebraic tools, in the next section we are going to address the case study given by the 9*j* (I,II).

2. Genesis of 9*j* Coefficients and Associated Diagrams

The 9*j* (I) coefficient (the "standard" 9*j*) can be written as a single sum of three 6*j* symbols (notations as in ref 5, Chapter 10 and Appendix 12). Note that the following expression can be looked at as the first instance of the recursion formula (1), namely this coefficient arises as a 3*nj* (I) for $n = 3$ starting from the unique $3(n-1)j$ with $n = 2$, i.e., from the 6*j* symbol itself

$$\sum_x (-)^{2x}(2x+1)\begin{Bmatrix} a & b & x \\ c & d & p \end{Bmatrix}\begin{Bmatrix} c & d & x \\ e & f & q \end{Bmatrix}\begin{Bmatrix} e & f & x \\ a & b & r \end{Bmatrix} = \begin{Bmatrix} a & f & r \\ d & q & e \\ p & c & b \end{Bmatrix} \quad (4)$$

where $\max\{|a-b|, |f-e|, |c-d|\} \le x \le \min\{a+b, f+e, c+d\}$.

The associated Yutsis diagram is

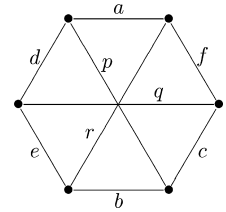

from which the triad structure as well as the symmetries of the coefficient are easily inferred (the six triads are associated with

3-valent nodes and correspond to columns and rows of the array; symmetries, up to phases, are implemented by odd or even permutations of columns or rows and the value of the coefficient does not change under transposition).

On applying type II recurrence formula (2) one should get a 9*j* (II) coefficient but it can be easily shown that the resulting configuration is a "trivial" one, being the product (without sum) of two 6*j*'s sharing a common triad

$$\sum_x (-)^{R+x}(2x+1)\begin{Bmatrix} a & b & x \\ c & d & p \end{Bmatrix}\begin{Bmatrix} c & d & x \\ e & f & q \end{Bmatrix}\begin{Bmatrix} e & f & x \\ b & a & r \end{Bmatrix} \doteq \begin{bmatrix} a & & d & & e \\ & p & & q & & r \\ b & & c & & f \end{bmatrix} = \begin{Bmatrix} p & q & r \\ e & a & d \end{Bmatrix}\begin{Bmatrix} p & q & r \\ f & b & c \end{Bmatrix} \quad (5)$$

The content of this formula is, however, highly nontrivial since it can be recognized as the Biedenharn−Elliott identity relating five 6*j* coefficients. (Recall that it represents, together with the orthogonality conditions, the "defining relation" of the hypergeometric polynomial of type ${}_4F_3$ associated with the 6*j*; see ref 5, p 295, and ref 11.)

The associated Yutsis diagram is clearly "separable" on the three lines *p*, *q*, *r*

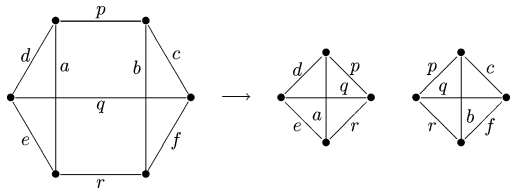

where on the right there appear two Yutsis diagrams of the 6*j* symbol, each to be thought of as a complete quadrilateral whose trivalent nodes correspond to triads of angular momentum variables according to the convention

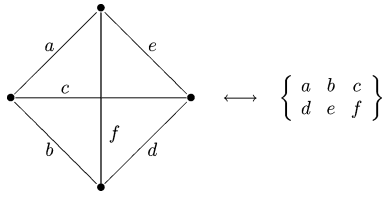

The two inequivalent ways of applying the Yutsis rule stated at the beginning of section 1, namely "inserting two nodes and joining them", generate in this simplest case two graphs isomorphic to the 9*j* (I) (left) and 9*j* (II) (right) diagrams

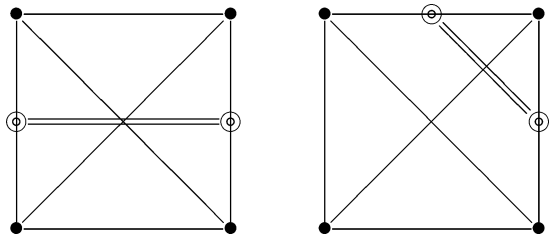

The explicit relationship between such a combinatorial procedure and the content of the algebraic recursion formulas (4) and (5) is postponed to section 3, where the insertion operations will be addressed in the 3*nj* (I,II) (any $n \geq 3$) cases and related to the general expressions given in (1) and (2).

2.1. Combinatorial Properties of 6*j* and 9*j* Graphs. In this section we are going to discuss properties of the simplest Yutsis graphs, which will be recovered in an improved way when addressing recursively 3*nj* (I,II) diagrams in section 3.

(a) The diagrams considered so far possess Hamiltonian circuits, as shown below.

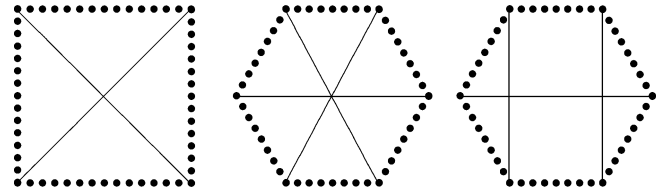

Recall that a Hamiltonian path in an undirected graph is a path that visits each vertex exactly once. A Hamiltonian cycle, or circuit, is a Hamiltonian path that returns to the starting vertex. Determining whether such paths and cycles exist in graphs is a typical instance of **NP**-complete problem.[8]

As will be shown in section 3, both 3*nj* graphs of type I and II admit by construction a Hamiltonian circuit of length 2*n* for all *n*, bounding a polygonal region ("plaquette") with the same number of sides (this is not necessarily true for other types of diagrams encountered for $n > 4$).

(b) Apart from Hamiltonian circuits, the diagrams possess other cycles bounding characteristic polygonal plaquettes. The drawings below display, for each diagram, a typical cycle of this kind (of course, owing to symmetries of the coefficients, other cycles of the same shape might have been depicted).

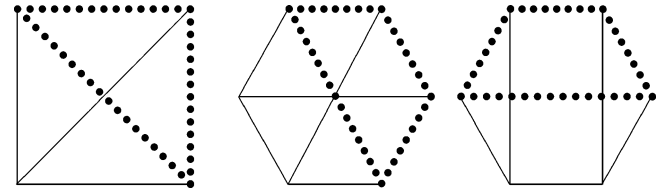

The number of edges $N_{\max}^{(n)}$ of the "largest", non-Hamiltonian circuit in a 3*nj* diagram depends only on *n* (there are only triangular plaquettes for $n = 2$ while there appear quadrilaterals for $n = 3$, pentagons for $n = 4$, etc., so that $N_{\max}^{(n)} = n + 1$). The 9*j* (II) graph actually contains also triangular circuits (not highlighted in the above picture) and this feature is related to the "separability" of this particular diagram as discussed above. Since the girth of a graph is defined as the length of the shortest cycle contained in the graph, the 9*j* (II) diagram is characterized by girth 3 while the 9*j* (I) has girth $4 = N_{\max}^{(3)}$.

Generally speaking, the presence of cycles with a number of edges strictly less than $N_{\max}^{(n)}$ is related to the separability of 3*nj* coefficients into a product (no sum) of lower order coefficients, namely to "trivial" configurations.

(c) The existence of circuits (Hamiltonian or not) can be assumed as a "guiding principle" in the search for asymptotic expansions of the 3*nj* coefficients by letting the edges belonging to the circuit become "large" while keeping "quantum" the others. This is what has been already done for the 6*j* in ref 13 for the 9*j* in ref 12, and

general results on the so-called phenomenon of "disentangling" of networks will be discussed in section 4 below.

(d) By resorting to notions from topological graph theory (see section 3), it is possible to classify Yutsis graphs associated with 3*nj* (I,II) diagrams according to the possibility of "embedding" them on closed surfaces.

Consider in particular the graphs of the 6*j* (to be classified as type II!) and of the 9*j* (II) (the separable one). They are both embeddable on a 2-sphere since they represent (the surfaces of) a tetrahedron and a triangular prism, respectively.

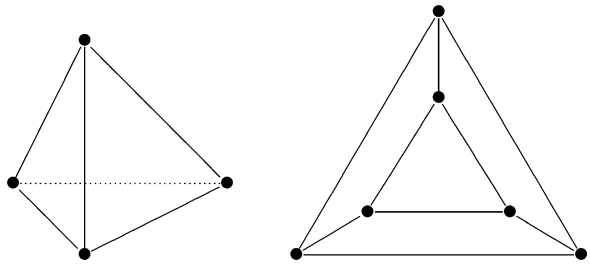

On the other hand, the 9*j* (I) diagram is a genus-1 or "toroidal" graph, as can be inferred by noting that this graph is isomorphic to $K_{3,3}$ (the bipartite graph on 6 nodes, or "utility graph"). To make this point explicit, recall that the torus T^2 can be thought of as a rectangle in the plane with opposite edges pairwise identified without twisting. The existence of a Hamiltonian circuit connecting all of the six nodes is crucial here: the circuit with its nodes is drawn as a horizontal straight line inside the rectangle and represents a longitudinal path on the torus (which is topologically a circle owing to identification of opposite points on vertical boundaries). The other connections are established in such a way that the connectivity of the original diagram is recovered (points to be identified pairwise have the same horizontal coordinates on the upper and lower boundaries).

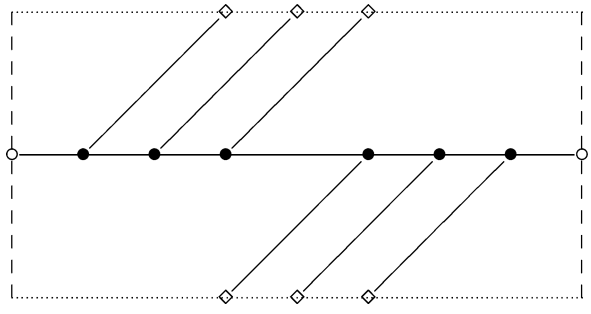

In section 3.2 the embedding of both 9*j* (I) and any other 3*nj* (I) diagram into the projective space will be addressed.

2.2. Recursion Relation for the 9*j* Symbol. According to remark (iii) of section 1, the starting point is the generating formula for a type I 3*nj* coefficient given in (1). It can be used to get an expression involving (sums of) products of two $3(n-1)j$ and four 6*j* as in (3). The explicit form of the latter in the present case reads (ref 5, p 345; the same in ref 2, p 175)

$$(-)^{a+f+b+j}\sum_x (-)^{2x}(2x+1)\times \begin{Bmatrix} a & b & x \\ d & e & f \\ g & h & j \end{Bmatrix}\begin{Bmatrix} a & b & x \\ c & \lambda & a' \end{Bmatrix}\begin{Bmatrix} j & f & x \\ \lambda & c & f' \end{Bmatrix} = (-)^{a'+f'+g+e}\sum_y (-)^{2y}(2y+1)\times \begin{Bmatrix} a' & b & c \\ y & e & f' \\ g & h & j \end{Bmatrix}\begin{Bmatrix} f' & e & y \\ d & \lambda & f \end{Bmatrix}\begin{Bmatrix} \lambda & d & a \\ g & a' & y \end{Bmatrix} \quad (6)$$

Specifying $\lambda = 1$, $a' = a$ and $f' = f$ and using explicit expressions for the 6*j* symbols, the above formula gives a five-term recursion relation for the 9*j* (ref 5 section 10.5.3, p 347; the same in ref 3, p 177), namely

$$\frac{\mathcal{A}_{c+1}(ab,fj)}{(c+1)(2c+1)}\begin{Bmatrix} c+1 & a & b \\ f & d & e \\ j & g & h \end{Bmatrix} + \frac{\mathcal{A}_c(ab,fj)}{c(2c+1)}\begin{Bmatrix} c-1 & a & b \\ f & d & e \\ j & g & h \end{Bmatrix} + \mathcal{C}(a,b,c,f,j)\begin{Bmatrix} c & a & b \\ f & d & e \\ j & g & h \end{Bmatrix} = \frac{\mathcal{A}_{d+1}(ef,ag)}{(d+1)(2d+1)}\begin{Bmatrix} c & a & b \\ f & d+1 & e \\ j & g & h \end{Bmatrix} + \frac{\mathcal{A}_d(ef,ag)}{d(2d+1)}\begin{Bmatrix} c & a & b \\ f & d-1 & e \\ j & g & h \end{Bmatrix} + \mathcal{D}(a,d,g,e,f)\begin{Bmatrix} c & a & b \\ f & d & e \\ j & g & h \end{Bmatrix} \quad (7)$$

where symmetries of the 9*j* have been used. The functions in front of the 9*j* coefficients are given explicitly by

$$\mathcal{A}_q(pr,st) = [(-p+r+q)(p-r+q)\times (p+r-q+1)(p+r+q+1)\times (-s+t+q)(s-t+q)(s+t-q+1)\times (s+t+q+1)]^{1/2} \quad (8)$$

$$\mathcal{C}(a,b,c,f,j) = \{[a(a+1)-b(b+1)+c(c+1)]\times [c(c+1)+f(f+1)-j(j+1)]\}/[c(c+1)] \quad (9)$$

$$\mathcal{D}(a,d,g,e,f) = \{[a(a+1)-d(d+1)-g(g+1)]\times [d(d+1)-e(e+1)+f(f+1)]\}/[d(d+1)] \quad (10)$$

The meaning of these quantities is geometrical, as happens in the three-term recurrence relation for the 6*j* symbol[9,1] (topic 9).[5] (Note, however, that the simplest derivation can be found in ref 14, where it was shown that only 6*j*'s where one of the entries is 1 are involved, as happens also here for the 9*j*.) In particular, $A_q(pr,st)$ represents the squared area of the quadrilateral bounded by *p*, *r*, *s*, *t* and made of two triangles meeting at *q*, while $\mathcal{C}$ and $\mathcal{D}$ are cosines of the dihedral angles at *c* and *d*, respectively (see ref 15 section 3 for more details). Each line in eq 7 closely resembles the structure of the recurrence formula of the 6*j*, the main difference being that here there are two running variables, (*c*, *d*) instead of

one (the other spins play the role of parameters). Notice that the entry labeled by h is not active, but we might write down a similar expression involving either the pair (c, h) or (d, h), and finally collect all of them in a seven-term relation in the three running variables c, d, h, as we are going to sketch below.

By introducing the shorthand notation

$$\begin{Bmatrix} c & a & b \\ f & d & e \\ j & g & h \end{Bmatrix} \doteq \mathcal{N}(c,d,h); \qquad \mathcal{C}(a,b,c,f,j) \doteq \tilde{\mathcal{C}}_c$$
$$\mathcal{D}(a,d,g,e,f) \doteq \tilde{\mathcal{D}}_d; \qquad \mathcal{H}(b,e,h,g,j) \doteq \tilde{\mathcal{H}}_h \tag{11}$$

where $\tilde{\mathcal{H}}_h$ represents the function to be associated with the third running variable, the complete recursion equation can be casted in the form

$$\tilde{\mathcal{A}}_{c+1}\mathcal{N}(c+1,d,h) + \tilde{\mathcal{A}}_c\mathcal{N}(c-1,d,h) + \tilde{\mathcal{C}}_c\mathcal{N}(c,d,h) =$$
$$\tilde{\mathcal{A}}_{d+1}\mathcal{N}(c,d+1,h) + \tilde{\mathcal{A}}_d\mathcal{N}(c,d-1,h) + \tilde{\mathcal{D}}_c\mathcal{N}(c,d,h) =$$
$$\tilde{\mathcal{A}}_{h+1}\mathcal{N}(c,d,h+1) + \tilde{\mathcal{A}}_h\mathcal{N}(c,d,h-1) + \tilde{\mathcal{H}}_h\mathcal{N}(c,d,h) \tag{12}$$

(the symbols $\tilde{\mathcal{A}}$ include the proper normalization factors defined as in (7)).

In the (triple) asymptotic limit $(c, d, h) \gg 1 \rightarrow (x, y, z)$ the "difference" equation above becomes a partial differential equation for the function $\mathcal{N}(x,y,z)$

$$[\Delta_x^2 - 2\cos\theta_x + 2]\mathcal{N}(x,y,z) =$$
$$[\Delta_y^2 - 2\cos\theta_y + 2]\mathcal{N}(x,y,z) = \tag{13}$$
$$[\Delta_z^2 - 2\cos\theta_z + 2]\mathcal{N}(x,y,z)$$

where Δ_x^2, Δ_y^2, Δ_z^2 denote second (partial) derivatives with respect to the continuous variables x, y, z while θ_x, θ_y, θ_z are angles whose cosines are defined in terms of both x, y, z and the other parameters of the original 9j coefficient. The derivation of each member of (13) can be carried out as in ref 10 and we refer the reader to ref 15 for details (see in particular their eq 22). However, in the present case the proper domain of the function $\mathcal{N}(x,y,z)$ is the Euclidean space $\mathbb{R}^3$ and $(\Delta_x^2, \Delta_y^2, \Delta_z^2) \equiv \Delta^2$ is the 3-dimensional Laplace operator. Moreover, if we equate each member of (13) separately to the same function $\mathcal{N}$ times a constant (to be determined), we would get a set of coupled eigenvalue equations, and the allowed values for the separation constant would generate the eigenvalue spectrum. Two more remarks are in order

(i) By setting $h = 0$ in (7), the conditions $b = e$ and $j = g$ follow necessarily. Then, according to remark iii and iv of section 1, we would see how the five-term recursion for the 9j simplifies for the 6j into a five-term recursion and thus, as we have just seen, in a two-variable difference equation which, in the asymptotic limit, leads to a two-dimensional coupled partial differential problem. Though such a procedure seems rather trivial because we already know that the 6j satisfied a three-term recurrence for which the "separation constant" is given, this point illustrates the "dual role" of, e.g., c and d, and the interest of studying the 6j symbol as a function of two variables at fixed values of the other four entries (see ref 13).

(ii) The above procedure, when applied to higher 3nj symbols, can be shown to lead to exactly n coupled equations in n variables for symbols of the first and second kind, and for highly symmetric ones, such as the 15j of the fifth type, whose Yutsis representation is the Petersen graph. Less symmetric cases might be dealt with according to the degree of their edge-transitivity.

More generally, such asymptotic techniques based on recurrence formulas—developed here for the 9j—represent the starting point for further developments concerning Rodriguez-type formulas (the defining differential relations of families of orthogonal polynomials; see refs 11 and 16 for 1-variable polynomials), recursion relations,[17] and their relationships with the issue of separability of Schrödinger equation in many-body quantum systems (see ref 15 and references therein). Apart from a short account in ref 16 (Chapter 5, section 4), such analysis in the case of two-variable orthogonal polynomials of hypergeometric type—as the 9j happens to be—seems to have been addressed only quite recently in the mathematical literature.[18] We argue that results we are going to review in section 4.1 on particular asymptotic expansions of the 9j and the novel general scheme for asymptotic disentangling of 3nj discussed in section 4.2 might contribute to shed light also on the generation of hierarchies of multivariable special functions of the hypergeometric type. Work is in progress in this direction.

3. Genesis of 3*nj* Diagrams

Looking at Yutsis diagrams as particular families of (unoriented) graphs, namely collections of nodes (vertices) and links (edges) connecting pairs of nodes, it is worth introducing a few notions and definitions from topological graph theory.[19]

A graph is embeddable on a surface Σ if its vertices and edges can be arranged on it without any crossing. The "genus" of a graph is the *lowest* genus of any surface on which the graph is embedded. Recall that closed and *orientable* surfaces Σ are topologically classified by their Euler number $\chi(\Sigma) = 2 - 2g$, where the genus g is the number of "handles" or "holes"; then $\chi = 2$ ($g = 0$, namely no handles) gives the two-sphere S^2, $\chi = 0$ ($g = 1$) gives the two-torus T^2 (whose presentation has been shown at the end of section 2.1), while the cases $g = 3, 4, \ldots$ correspond to double, triple, ... torus Σ_g, all characterized by an even negative χ. A planar graph is one that can be drawn on the Euclidean plane or, *equivalently*, on the sphere S^2 without any crossing, namely, it is has genus 0 or $\chi = 2$.

The issue of the classification of Yutsis graphs is a longstanding problem[1,20] and in particular such a "topological" viewpoint has been addressed in ref 21. In this section we are going to complete the characterization of all 3nj (I,II) diagrams by resorting to the analysis of the combinatorial and topological contents of the "insertion operations" in connection with the recurrence formulas (1) (type I) and (2) (type II). Moreover, the existence of Hamiltonian cycles (defined below) in any of such diagrams will be the starting point of the analysis of asymptotic disentangling developed in section 4. Finally, a few remarks on the application of our recursive procedure to other types of 3nj diagrams are briefly discussed.

We start from the analysis of type-II graphs since they share simpler features.

3.1. 3*nj* (II) Diagrams. ***Proposition 1.*** *Any* 3nj *diagram of type II is planar (or genus-0).*

Recall from section 2.1 that both the 6j (tetrahedron) and the 9j (II) (triangular prism) graphs are easily recognized as planar.

Comparing the original diagrams up to the 18*j* given in refs 2 and 3 reveals that a convenient and unified way of drawing all 3*nj* (II) is through Schlegel diagrams of prisms based on polygons with an increasing number of sides. Below the square (12*j*), pentagonal (15*j*), and hexagonal (18*j*) prisms of this sort are depicted, while the triangular prism associated with the 9*j* (I) has been already shown at the end of section 2.1.

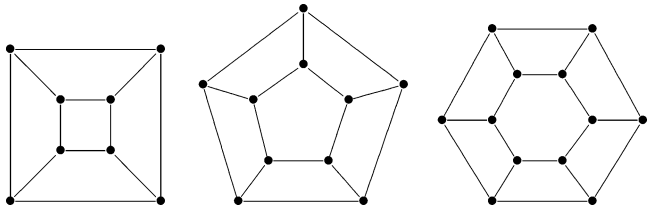

Every 3*nj* (II) has a Hamiltonian circuit of length 2*n*, as can be easily inferred from the two samples shown below.

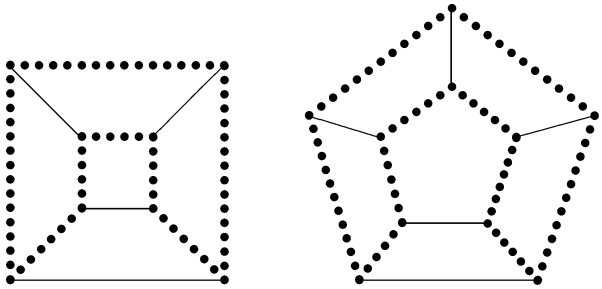

Other non-Hamiltonian cycles of increasing length appear as well, and it turns out that the girth number (the length of the shortest cycle) is exactly 4 for all of these graphs (recall that the property of having girth 3, namely the existence of triangular circuit(s) implies separability of the diagram into lower order diagrams and as such has been already ruled out, cf. the recursion rule stated at the beginning of section 1).

Proposition 2. *There exists (up to symmetry) one kind of insertion operation, denoted by* $\mathcal{T}_{\square}$*, that generates the 3nj (II) from the* $3(n-1)j$ *(II) for any* $n \geq 3$ *according to the recurrence formula (2). Moreover* $\mathcal{T}_{\square}$ *is topology-preserving, namely all graphs derived in such a way stay planar.*

The proof can be carried out by resorting inductively to the Yutsis graphical method, which mimics step-by-step algebraic manipulations to be performed on equations. The figures below deal with the generation of the 12*j* (II) from the 9*j* (II) and make it manifest the effective equivalence between the combinatorial recursion method and the algebraic recurrence formula.

In the first figure the recursion rule "add two vertices and join them" (pictorially ◎ = ◎) is applied on any one of the lateral faces of the triangular prism.

In the second one the content of the algebraic recurrence formula (2) for 3*nj* (II), $n = 3$, is displayed: the summation over x implies the cancellation of both edges labeled by x and nodes which lose an incident edge; in the last step edges with the same labels are joined again to give the final closed diagram.

Note that the two diagrams of the 9*j* (II) on the left-hand side of each picture are isomorphic, as well as the two resulting graphs of the 12*j* (II) on the right-hand sides.

The diagrammatic (box-like) and algebraic forms of the insertion operator to be used recursively for the generation of any 3*nj* (II) diagram or associated coefficient are summarized

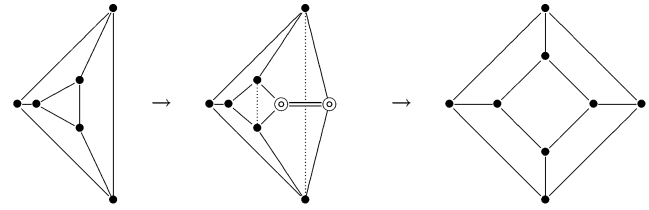

Combinatorial recursion rule (type II)

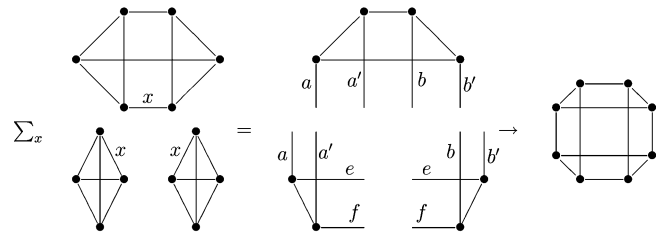

Algebraic recurrence formula $9j(\mathrm{II}) \rightarrow 12j(\mathrm{II})$

in the following table (where the factor $(2x + 1)$ and a phase have been dropped)

$$\mathfrak{I}_{\square} \leftrightarrow \begin{array}{ccccc} a & & e & & b \\ & d & & c & \\ a' & & f & & b' \end{array} \leftrightarrow \sum_x \begin{Bmatrix} a & b & x \\ c & d & e \end{Bmatrix} \begin{Bmatrix} a' & b' & x \\ c & d & f \end{Bmatrix}$$

Because such an insertion can be applied by construction without changing the intrinsic topology (any prism with basis an n-gon is changed into a prism with basis an $(n + 1)$-gon) the proof of Proposition 2 is completed.

3.2. 3*nj* (I) Diagrams. Looking at samples of 3*nj* (I) diagrams as depicted in refs 2 and 3, one can easily infer that all of them are "cartwheel" configurations, labeled consistently as shown below (the arrangement of labels complies with the right-hand side of (1))

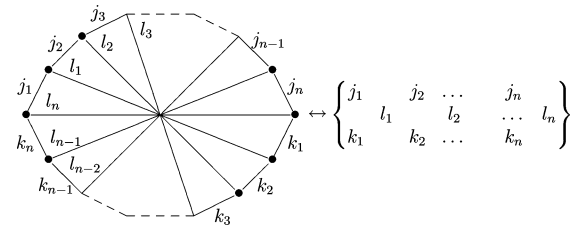

Recall that the computation of the Euler number χ of a connected configuration of nodes and links drawn in the plane can be performed by evaluating the quantity $V - E + F$ ($V =$ number of vertices, $E =$ number of edges, $F =$ number of faces). Here a "face" is any region of the plane bounded by some polygonal contour with a certain number of vertices, but graphs with multiple edge-crossings, as those in the previous picture, must be suitably rearranged to get the correct counting. To such a number must be added 1 to take in account the "external" region, namely the portion of the plane not included into the graph.

Proposition 3. *Any 3nj diagram of type I is a graph with Euler number* $\chi = 1$.

The proof proceeds by induction on n and will be completed after Proposition 4. According to the definition given in the introduction to this section, it is worth noting preliminarily that

a Euler number equal to 1 does not correspond to any embedding of graphs on an *oriented* surface. Actually, the definition of χ can be generalized to (embeddings of graphs on) *nonorientable* closed surfaces $\tilde{\Sigma}$ by introducing the so-called "crosscap number" c, namely the number of Möbius bands one must attach to the sphere S^2 to obtain the desired surface. Such a "nonorientable genus" is related to the Euler number of $\tilde{\Sigma}_c$ by $\chi(\tilde{\Sigma}_c) = (2 - c)$ and $\chi = 1$ corresponds to the (minimum) crosscap number $c = 1$ characterizing the real projective plane P ($\mathbb{RP}^2$ in the standard mathematical notation).

The $9j$ (I) diagram was explicitly shown to be embeddable in P in ref 9 but this feature is actually well-known because of its isomorphism with the complete bipartite graph $K_{3,3}$ (see, e.g., ref 19).[22]

Taken for granted this result, the following Proposition deals with the existence of a well-defined insertion operation characterized by the fact that it preserves the Euler number, namely the variation $\Delta_{n-1,n}\chi$ of χ in passing from $3(j - 1)$ (I) to $3nj$ (I) diagrams is zero.

Proposition 4. *There exists (up to symmetry) one kind of "twisted" insertion operation, denoted by $\mathscr{T}_{\bowtie}$, that generates the $3nj$ (I) from the $3(n - 1)j$ (I) for any $n \geq 3$ according to the recurrence formula (1). Moreover, $\mathscr{T}_{\bowtie}$ is topology-preserving with respect to embeddings in P.*

The proof can be carried out by resorting to the graphical method as already done in section 3.1 for type II diagrams. In the figure below the generation of the $3nj$ (I) from the $3(n - 1)j$ (I) according to the algebraic recurrence formula (1) is shown. The summation over x implies the cancellation of both edges labeled by x and nodes which lose an incident edge; the last step would consist of joining back edges with the same labels to get the $3nj$ (I) diagram represented at the beginning of this section. Note that, up to relabeling, the same construction could be performed on anyone of the $(n - 1)$ rays of the $3(n - 1)j$ (I) and the resulting coefficients have the same values owing to their symmetry properties.[2]

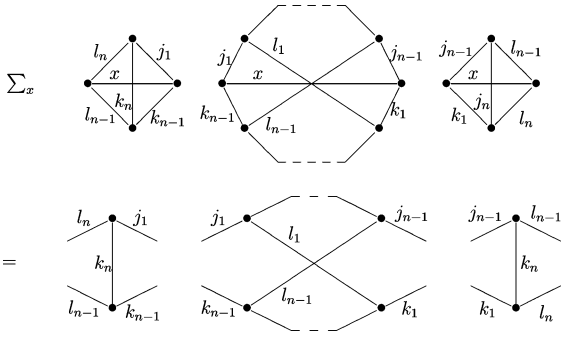

The diagrammatic [algebraic] form of the twisted insertion operator $\mathscr{T}_{\bowtie}$ to be used recursively for the generation of any $3nj$ (I) diagram [coefficient] is summarized in the following table (where the factor $(2x + 1)$ and a phase have been dropped).

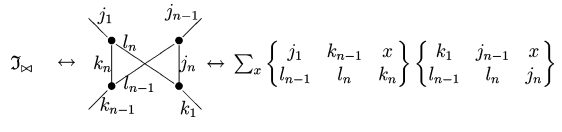

The topological invariance of such an operation is easily proved by observing that the variation of the Euler number owing to one insertion is given by

$$\Delta_{n-1,n}\chi[\mathscr{T}_{\bowtie}] = \Delta V - \Delta E + \Delta F = 2 - 3 + 1 \equiv 0 \tag{14}$$

where ΔV is the number of new vertices, ΔE is the number of new edges, and ΔF is the number of new faces. (Recall that any type of $3nj$ diagram has $2n$ vertices and $3n$ edges and note that the $(n + 1)$ "faces" for type I can by quickly selected by looking at the n cycles that include each of the n rays and adding $+1$ for the external region.)

Now the proof of Proposition 3 can be completed by induction. Given that $\chi[9j] = 1$ and assuming $\chi[3(n - 1)j] = 1$, by (14) we get

$$\chi[3nj] = \chi[3(n - 1)j] + \Delta_{n-1,n}\chi[\mathscr{T}_{\bowtie}] = 1 \tag{15}$$

for any $n \geq 3$.

A comment is in order about the possibility of generating recursively the other types of $3nj$ diagrams arising for $n > 4$.[2,3] We argue that, on applying suitable sequences of N insertion operations $\mathscr{T}_{\square}$ (Proposition 2) and $\mathscr{T}_{\bowtie}$ (Proposition 4) starting from the simplest graph, namely, the complete quadrilateral associated with the $6j$, *all types* of $3(2 + N)j$ diagrams can be generated. Actually the topological invariance proved in the two propositions holds true only when $\mathscr{T}_{\square}$ is applied to a type II diagram (and similarly $\mathscr{T}_{\bowtie}$ to a type I diagram) under the circumstances described above. However, different positions of the insertions and/or actions on the other type of diagrams would provide a variety of configurations with possible changes of the underlying topology. Work is in progress in this direction.

In view of applications to be addressed in the following we conclude this section by noticing that every $3nj$ (I) diagram has a Hamiltonian circuit of length $2n$, as the samples of $12j$, $15j$, and $18j$ (I) shown below make it manifest. The Hamiltonian cycle would be always consistently labeled by the ordered set $j_1, j_2, ..., j_n, k_1, k_2, ..., k_n$ and the rays by $l_1, l_2, ..., l_n$.

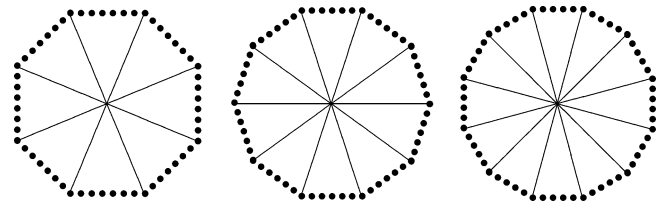

Other non-Hamiltonian cycles appear as well in these diagrams. There are both cycles of length equal to $n + 1$ (including one ray and n edges on the perimeter) as well as cycles of length equal to the girth number, which is 4 for each n as already happened for $3nj$ (II) diagrams (now these 4-cycles are associated with "twisted" configurations of four edges labeled cyclically by k_i, j_i, l_{i-1}, l_i).

4. Asymptotic Disentangling of 3*nj* Diagrams

In two previous papers[23,24] the mathematical apparatus of angular momenta recoupling theory[1] (topic 12) has been shown to provide a unifying background structure for a number of phenomena and applications ranging from atomic, molecular, and nuclear physics to quantum computing and gravity (cf. also ref 25). The term *spin networks*, originally introduced by Penrose[26] in connection with a model combinatorial spacetime, was used as a synonym of $3nj$ diagrams, namely connected and closed regular graphs whose $2n$ nodes are associated with triads

of angular momentum variables, each satisfying triangle inequality. By *semiclassical* spin networks we mean, as in refs 23 and 24, those families of 3*nj* diagrams that arise when all or just a few of the 3*n* spin variables become large (namely the angular momentum labels attached to them are $\gg 1$ in $\hbar$ units). The issue of semiclassical analysis of angular momentum quantum transition amplitudes dates back to the beginning of quantum mechanics, and we do not insist here on the wide range of applications of such techniques. Rather, we are going to reach a general assessment starting from what has been done for the 9*j* symbol in ref 12, where the case in which six edges become large was shown to provide the *disentangling* of the underlying network, in the sense explained in section 4.1 below. (Note that a more formal approach based on geometric quantization techniques for both 3*j* (Wigner) coefficient[27] and 6*j* symbol[15] can be carried out as well.)

Whatever kind of asymptotics we want to address, the first object to be analyzed is the three-valent node itself, namely the basic building block of any 3*nj* diagram. Given that a node is naturally associated with a 3*j* (Wigner) coefficient, and forgetting its dependence on magnetic quantum numbers, we summarize the possible choices of small/large angular momentum values in the following picture, where solid lines and small letters stand for truly "quantum" labels while capital letters and double dotted lines represent "semiclassical" large values.

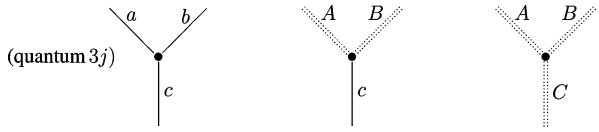

Here we recover graphically the admissible asymptotics for 3*j* coefficients, that is, "if one spin value is large then at least one of the other incident spins must be large as well". Moreover, if the right-hand case (3, 0) occurs at any one of the 2*n* nodes of a 3*nj* diagram, the resulting configuration turns out to be related to an amplitude whose distribution represents (a suitable number of) decoupled harmonic oscillators. Thus the "quantum entanglement of states", measured precisely by the transition amplitudes associated with 3*nj* coefficients, is lost when approaching the classical limit, namely when the underlying quantum system undergoes a complete decoherence.

The prototype of this phenomenon was addressed in the famous paper by Ponzano and Regge[9] on the "Semiclassical limit of Racah coefficients" dealing with the simplest spin network, the 6*j* symbol itself. In what follows we are going to explore and classify asymptotic regimes in which different kinds of "asymptotic disentangling" arise in configurations that include (2, 1)-nodes. (Recall that the well-known formulas for the (3, 3) and (4, 2) 6*j* cases, corresponding to the cycles shown in section 2.1, are listed as eqs 2 and 3 in ref 12).

As a case study we review first the main results on the 9*j* (I) proved in ref 12 by supporting them with new numerical simulations.

4.1. The 9j Case. The focus of this section is on the 9*j* (I) symbol, well-known in atomic spectroscopy for its role as the matrix element of the transformation between *LS* and *jj* coupling schemes, but exhibiting features prototypical of more complex spin networks. In quantum chemistry, it appears for example in matrix elements when Sturmian or momentum space orbitals are employed.[28] On the basis of the remarks at the end of section 2.2, it is worth noting that the physical situations where some of the angular momenta become large, correspond mathematically to the case of discrete functions becoming continuous in the limit, as we are going to check in what follows. Note, however, that we are not going to address the analog of Ponzano−Regge asymptotics (9 entries of the 9*j* large, or (9, 0) expansion) and refer the reader to ref 5 section 10.7 for details (the same reference is the basic one for notations and algebraic expressions used in this section).

All cases where some entries are large and some small can be reduced to the (4, 5) or "large corner" case and to the (6, 3) or "small diagonal" case by permutation symmetries. The associated Yutsis graphs with dotted edges representing large entries are

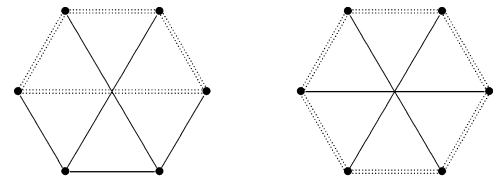

Recall that the basic expression of the 9*j* as a sum over *x* of the product of three 6*j* was already given in (4). By slightly changing spin labels to comply with notations in ref 12, we rewrite it as

$$\sum_x (-)^{2x}(2x+1)\begin{Bmatrix} a & b & c \\ f & i & x \end{Bmatrix}\begin{Bmatrix} d & e & f \\ b & x & h \end{Bmatrix}\begin{Bmatrix} g & h & i \\ x & a & d \end{Bmatrix} = \begin{Bmatrix} a & b & c \\ d & e & f \\ g & h & i \end{Bmatrix} \quad (16)$$

where $\max\{|a-i|,|b-f|,|h-d|\} \le x \le \min\{a+i, b+f, h+d\}$.

The (6, 3) asymptotic case is derived from this defining equation by suitably applying the well-known (3, 3) expansions for the 6*j*,[9,10] and the final result reads (recall that capital letters stand for large entries)

$$\begin{Bmatrix} a & B & C \\ D & e & F \\ G & H & i \end{Bmatrix} \xrightarrow{(6,3)} \frac{(-)^{B+H-e}}{\Gamma_1\Gamma_2}\, \mathbf{d}^{a}_{C-B,G-D}(\cos\theta)\, \mathbf{d}^{i}_{F-C,H-G}(\cos\theta) \quad (17)$$

where there appear two Jacobi polynomials (Wigner **d**-matrices of a cosine), with principal quantum numbers *a*, *i* (two of the "small" entries) and argument given by

$$\cos\theta = \frac{(2e+1)^2 - (B+F+1)^2 - (D+H+1)^2}{2(B+F+1)(D+H+1)}$$

Note that the role of magnetic quantum numbers in $\mathbf{d}^{j}_{MM'}$ is played here by differences of "large" spin variables that vary consistently between $-j$ and $+j$ in integer steps. Finally, the multiplicative factors Γ read

$$\Gamma_1 = \left\{\left[\frac{2}{3}(B+C+f)+1\right]\left[\frac{2}{3}(D+G+H)+1\right]\right\}^{1/2}$$
$$\Gamma_2 = [(B+F+1)(D+H+1)]^{1/2}$$

The (4, 5) case was addressed years ago by Watson[29] and his results are summarized in

$$\begin{Bmatrix} A & b & C \\ d & e & f \\ G & h & I \end{Bmatrix} \xrightarrow{(4,5)} \frac{(-)^{b+C-d-G}}{2X+1} \begin{pmatrix} b & e & h \\ C-A & \epsilon & G-I \end{pmatrix} \times \begin{pmatrix} d & e & f \\ G-A & \epsilon & C-I \end{pmatrix} \quad (18)$$

where there appear two Wigner 3*j* symbols and $X = {}^1/_4(A + C + G + I)$, $\epsilon = A - C - G + I$.

Both formulas can then be taken as an illustration of "disentangling" of the associated 9*j* networks because in the above semiclassical limits no summation ("superposition") appears anymore. Both **d**-matrices and Clebsch−Gordan (Wigner) coefficients represent well-defined classes of orthogonal polynomials belonging to the Askey hierarchy, as illustrated for instance in ref 15 in connection with the quantum theory of angular momentum. As is well-known, the issue of separability of variables in quantum mechanics is associated, by group theoretical arguments, with continuous or discrete symmetries and allows the expression of wave functions of a composite system as a product of wave functions of subsystems. On the other hand, nonseparability requires introduction of coupling by expanding on a linear combination of a set of such basis wave functions. Interpreting the original expression of the 9*j* given in (4) (or in (16)) as an expansion of a global "spin network" wave function, where the entries are discrete variables, the asymptotics (17) and (18) actually lead to wave functions proper of separated systems (note that the surviving angular momentum functions depend on both truly quantum discrete variables and on semiclassical, continuous ones). Indeed, from the analysis carried out in section 2.1, we see that the variables are explicitly designated by *c*, *d*, and *h* in the discrete case of a coupled set of difference equations, and by *x*, *y*, and *z* in the continuous limit of a coupled set of partial differential equations. This appears to have been anticipated in an early remark by Neville.[14]

From the graphical viewpoint, what is left after "deletion" of the dotted edges (associated with real-valued variables that tend to infinity) is in both cases a graph with no more closed cycles and thus "trivial". They look like isolated edges (case (6, 3)) or tree configurations (case (4, 5)), which are both topologically "contractible". The "entangled" nature of higher 3*nj* cases can be discussed along similar lines and according to remark ii of section 2.2. In the next section we are going to deal systematically with their disentangling. Note finally that such disentangling phenomena might be discussed and interpreted from many other viewpoints since spin network graphs (3*nj* diagrams) are encountered in quantum gravity models, discrete mathematics, and quantum computing (refs 23−25 and reference therein). We plan to investigate new applications of our asymptotic techniques in these contexts.

Further important insight on disentangling may come from computational studies. In ref 12 Wigner **d**-functions, Clebsch−Gordan coefficients and other special functions were calculated by directly summing their defining series using multiprecision arithmetic (MPFUN90).[30] The multiple precision arithmetic allows convenient calculation of hypergeometric functions, of small and large argument by their series definition, and without the necessity of using recurrence relations, integral and rational representations, or asymptotic approximations. On the basis of definining relations and formulas for the functions given in various chapters of ref 5, the basic problem encountered in these summations is that some of the terms in the sum may become very large ($\sim 10^{100}$ or larger). However, the sum must be a number in a small finite range, e.g., [−1, +1], and normal computer precision (8−32 decimal places) will not generally produce accurate summation. On the other hand, multiple precision arithmetic packages that allow calculations with thousands (or millions!) of digits sum the hypergeometric series easily for a spin variable *j* of magnitude much larger than 1000.

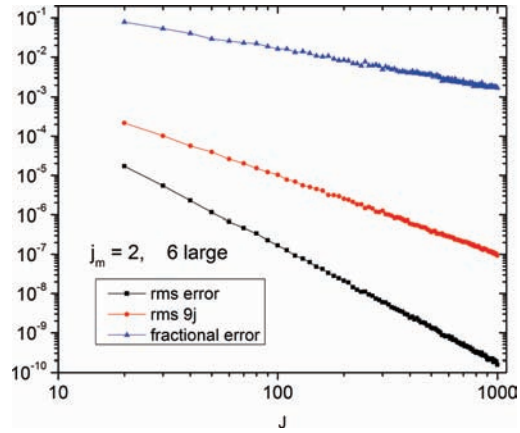

Figure 1. rms (root mean square) deviation of the approximate 9*j* from the exact value, the rms magnitude of the 9*j*, and the fractional error (given by their ratio) plotted for $jm = 2$ and 6 large entries.

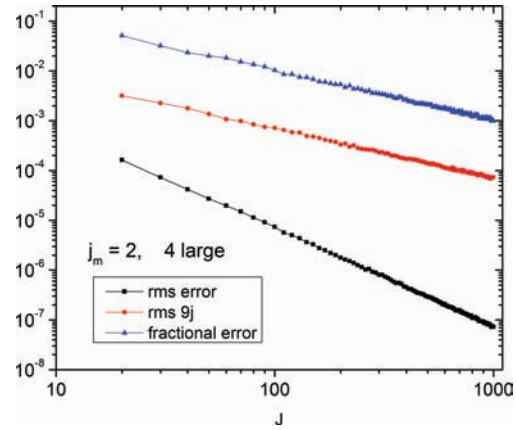

Figure 2. rms (root mean square) deviation of the approximate 9*j* from the exact value, the rms magnitude of the 9*j*, and the fractional error (given by their ratio) plotted for $jm = 2$ and 4 large entries.

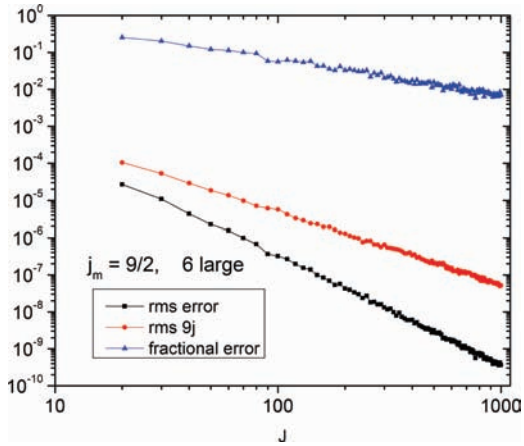

Figure 3. rms (root mean square) deviation of the approximate 9*j* from the exact value, the rms magnitude of the 9*j*. and the fractional error (given by their ratio) plotted for $jm = 9/2$ and 6 large entries.

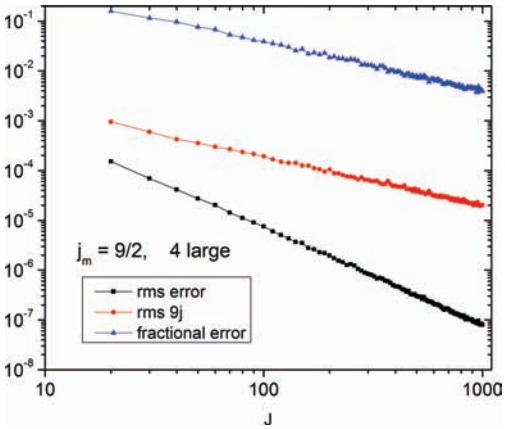

Figure 4. rms (root mean square) deviation of the approximate 9*j* from the exact value, the rms magnitude of the 9*j*, and the fractional error (given by their ratio) plotted for $jm = 9/2$ and 4 large entries.

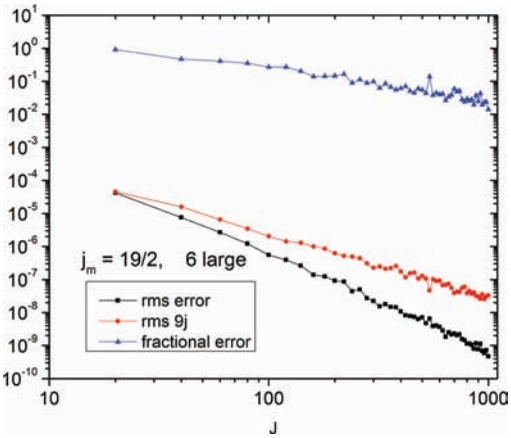

Figure 5. rms (root mean square) deviation of the approximate 9*j* from the exact value, the rms magnitude of the 9*j*, and the fractional error (given by their ratio) plotted for $jm = 19/2$ and 6 large entries.

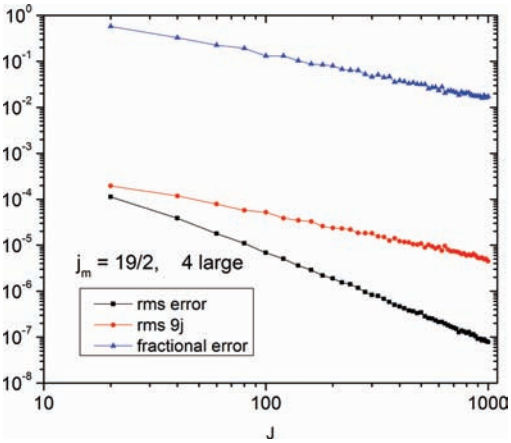

Figure 6. rms (root mean square) deviation of the approximate 9*j* from the exact value, the rms magnitude of the 9*j*, and the fractional error (given by their ratio) plotted for $jm = 19/2$ and 4 large entries.

The asymptotic formulas (17) and (18) have been already tested in ref 12 by calculating 9*j* symbols and their approximations for huge randomly selected sets of *j* values, but we conclude this section by presenting new numerical experiments, illustrated in the following and displayed in the figures below.

The large entries on the coefficients (either 6 or 4 according to either (17) or (18)) have values ranging from a given abscissa, J to $J + j_m$, where J is chosen between 20 and 100. The small *j* (integer and half-integer) values are randomly selected from

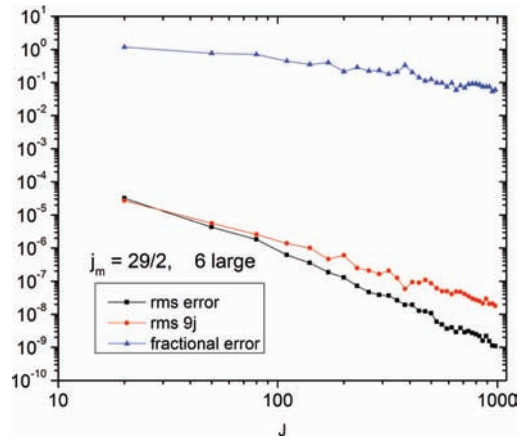

Figure 7. rms (root mean square) deviation of the approximate 9*j* from the exact value, the rms magnitude of the 9*j*, and the fractional error (given by their ratio) plotted for $jm = 29/2$ and 6 large entries.

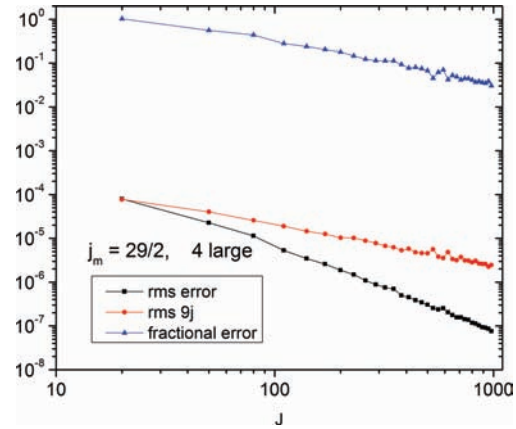

Figure 8. rms (root mean square) deviation of the approximate 9*j* from the exact value, the rms magnitude of the 9*j*, and the fractional error (given by their ratio) plotted for $jm = 29/2$ and 4 large entries.

the range $[0, j_m]$. The calculations use 1000 nonzero 9*j* values for each J and integer and half-integer small *j* for $j_m = 2, 9/2, 19/2, 29/2$. We calculate the *rms deviations*, i.e., the root-mean-square deviations of the approximate 9*j* from the exact values, and the *rms magnitudes* of the 9*j* symbols. We take the ratio of these quantities to evaluate the *fractional error* in the disentangled 9*j* symbol. Then the numerical experiments show that the fractional error decreases as J^{-1} for both eqs 17 and 18) while the rms magnitudes decrease as J^{-2} for eq 17 and J^{-1} for eq 18).

Experiments with different values for j_m show that the fractional errors for both equations scale as j_m^2/J. For the six large angular momenta formula, the fractional error is approximately $0.3j_m^2/J$. For the four large angular momenta formula, the fractional error is approximately $0.2j_m^2/J$. The Watson equation (18) produces a significant number of zero values (15−20%) for small but nonzero exact 9*j* symbols. These zeros result from combinations of angular momenta that yield zero values for the 3*j* symbols. Preliminary numerical checks indicate a correlation with the previously mentioned phenomenon of the appearance of nodes in separable conditions. Remarkably the rms magnitudes of the 9*j* symbols that correspond to zero approximate values scale as J^{-2} and have approximately the same values as the rms deviation values. Hence the quality of the overall approximation is not degraded even if the cases with zero approximate values are included.

4.2. General Case. Recall from section 3 that both 3*nj* (I) and 3*nj* (II) spin networks possess a Hamiltonian circuit of

length $2n$. In this section we are going to show how disentangling (induced by letting the $2n$ spin variables on this closed cycle to become large) works for any $3nj$ diagram of type I by applying recursively an asymptotic version of the insertion operation $\mathcal{T}_{\bowtie}$ (a similar procedure might be set up for $3nj$ (II)).

To make the notation used in section 4.1 compatible with the general case, let us rewrite the $9j$ (I) accordingly in terms of the labels $\{j, k, l\}$ (see (1) and the diagram of the $3nj$ (I) at the beginning of section 3.2). Consider at the same time the limit in which the Hamiltonian cycle (the external circle of the cartwheel diagram with three internal edges) is labeled by large spin values, denoted by capital letters

$$\begin{Bmatrix} j_1 & & j_2 & & j_3 & \\ & l_1 & & l_1 & & l_1 \\ k_1 & & k_2 & & k_3 & \end{Bmatrix} \xrightarrow{j_1,j_2,j_3,k_1,k_2,k_3 \gg 1} \begin{Bmatrix} J_1 & & J_2 & & J_3 & \\ & l_1 & & l_1 & & l_1 \\ K_1 & & K_2 & & K_3 & \end{Bmatrix} \quad (19)$$

To such a (6, 3) expansion of the $9j$ (6 large, 3 small entries) we can apply the general twisted insertion operation defined in Proposition 4 of section 4.2 to get the $12j$ (I). In the present case, without imposing any restriction on the entries, it would read

$$\mathcal{T}_{\bowtie} \leftrightarrow \sum_x \begin{Bmatrix} j_1 & k_3 & x \\ l_3 & l_4 & k_4 \end{Bmatrix} \begin{Bmatrix} k_1 & j_3 & x \\ l_3 & l_4 & j_4 \end{Bmatrix} \quad (20)$$

However, since such a combination has to be "coupled" with the (6, 3) $9j$ (in which an x takes formally the place of the "small" l_3 in (19)) we see that the entries j_1, k_3, k_1, j_3 are necessarily "large" because they lie on the preexisting Hamiltonian great circle, while l_3 stays small. Then we are left with the residual problem of determining the order of magnitude of the new entries j_4, k_4, l_4 (recall that x is small). This is achieved by checking the triads of the two $6j$ symbols in (20) to see which possibilities we have for these three labels in view of the admissibile configurations for the $3j$ coefficient discussed in the introduction to this section.

• The triads of $\begin{Bmatrix} J_1 & K_3 & x \\ l_3 & l_4 & k_4 \end{Bmatrix}$ are

$(J_1\ K_3\ x)$ (2 large, 1 small) and as such it is admissible;

$(l_3\ l_4\ x)$ (2 small) and thus l_4 must be small;

$(J_1\ l_4\ k_4)$ (1 large, 1 small) and then k_4 must be large and renamed K_4;

$(l_3\ K_3\ K_4)$ (2 large, 1 small) and then admissible.

• The triads of $\begin{Bmatrix} K_1 & J_3 & x \\ l_3 & l_4 & j_4 \end{Bmatrix}$ are

$(K_1\ J_3\ x)$ (2 large, 1 small) and as such it is admissible;

$(l_3\ l_4\ x)$, which is the same triad considered before;

$(K_1\ l_4\ j_4)$ (1 large, 1 small) and then j_4 must be large and renamed J_4;

$(l_3\ J_3\ J_4)$ (2 large, 1 small) and then admissible.

Since the above remarks clearly hold true for any insertion operation which acts on a preexisting [$2(n-1)$ large, $(n-1)$ small] $3(n-1)j$ (I) diagram, we have established the following.

Proposition 5. *There exists (up to symmetry) one kind of twisted "asymptotic" insertion operation, denoted by* $\mathcal{T}^{as}_{\bowtie}$*, that generates a unique Hamiltonian disentangled* $(2n, n)$ $3nj$ *(I) diagram from the similar* $[2(n-1), (n-1)]$ $3(n-1)j$ *(I) for any* $n \geq 3$.

Its general (graphical and algebraic) expression reads

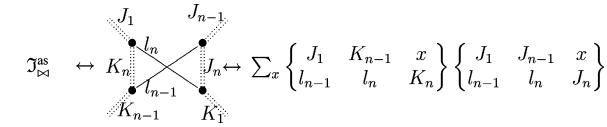

$$\leftrightarrow \sum_x \begin{Bmatrix} J_1 & K_{n-1} & x \\ l_{n-1} & l_n & K_n \end{Bmatrix} \begin{Bmatrix} J_1 & J_{n-1} & x \\ l_{n-1} & l_n & J_n \end{Bmatrix}$$

where edges with large labels are drawn as dotted lines.

Thus we can easily infer that, on the basis of the (6, 3) expansion of the $9j$ given in (17), the analytical expression of any Hamiltonian asymptotic expansion of a $(2n, n)$ $3nj$ (I) diagram contains the product (no sum) of $(n-1)$ Wigner **d**—functions whose principal quantum numbers may be chosen among the n spin variables $\{l_1, l_2, ..., l_n\}$ (a similar result can be established for $3nj$ (II) diagrams).

5. Conclusions and Outlook

We have developed in this paper a recursive procedure for the generation of $3nj$ from $3(n-1)j$ diagrams of types I and II as well as an original approach to the classification of their asymptotic disentangling.

There are a number of open questions that deserve further investigations.

The recursive generation of all other types of $3nj$ diagrams would be a major achievement, as pointed out already in ref 1 (topic 12). We argue that it would be possible (at least in principle) to complete the enumeration of diagrams of type III, IV, V, ... for any $n > 4$ starting from either type I or II and applying suitably chosen sequences of the two kind of insertion operators defined in section 3. However it should be clear that the enumeration will blow up as n increases and the hardest task will be to rule out isomorphic configurations (see refs 7 and 20).

For what concerns semiclassical limits and asymptotic disentangling, we are currently performing numerical experiments on the five types of $15j$ coefficients to test the relative magnitudes and associated probabilities (cf. ref 31 for an early attempt of comparison between types I and II). We have restricted most of the treatment in section 4 to Hamiltonian circuits, but it can be conjectured that the described features of disentangling will occur for other circuits in general spin networks. It would be also interesting to analyze the different asymptotic regimes in connection with the symmetry properties of the different types of coefficients.

An improvement of multivariable recursion relations and related partial differential equations (see the $9j$ case discussed in section 2.2) would greatly help in providing further insights in the classification of the associated orthogonal polynomials of hypergeometric type.

The results obtained here, as well as possible new improvements along the lines outlined above, represent a prerequisite for extending to $3nj$ the analysis based on sophisticated (quantum and semiclassical) geometric and analytical techniques introduced in refs 13 and 27; see also ref 32.

Acknowledgment. We are very pleased to coauthor this paper with Professor Vincenzo Aquilanti in this issue in honor of his seventieth birthday. We join in celebrating his remarkable career in theoretical and experimental chemistry.

References and Notes

(1) Biedenharn, L. C.; Louck, J. D. The Racah-Wigner Algebra in Quantum Theory. *Encyclopedia of Mathematics and its Applications Vol 9*; Rota, G.-C., Ed; Addison-Wesley Publ. Co.: Reading, MA, 1981.

(2) Yutsis, A. P.; Levinson, I. B.; Vanagas, V. V. *The Mathematical Apparatus of the Theory of Angular Momentum*; Israel Program for Sci. Transl. Ltd.: Jerusalem, 1962.

(3) Yutsis, A. P.; Bandzaitis, I. B. *Angular Momentum Theory in Quantum Mechanics*; Mokslas: Vilnius, 1965 (in Russian).

(4) Zare, R. N. *Angular Momentum*; Wiley: New York, 1988.

(5) Varshalovich, D. A.; Moskalev, A. N.; Khersonskii, V. K. *Quantum Theory of Angular Momentum*; World Scientific: Singapore, 1988.

(6) The last two monographs were published seven years after the Biedenharn-Louck text; in particular the last one is now the most exhaustive and reliable collection of definitions of angular momentum functions and related algebraic and analytic formulas.

(7) As an aside remark, recall that the isomorphism problem in graph theory is a typical **NP**-complete problem, actually a **#P** problem, even for regular graphs: this means that, given two instances of graphs, one can decide if they are isomorphic or not in polynomial time but the general solution -the enumeration of all graphs isomorphic to a given one- requires an exponential time as the complexity of the graphs grows, i.e., as the number of vertices increases (see, e.g., ref 8).

(8) Garey, M. R.; Johnson, D. S. *Computers and Intractability: A Guide to the Theory of NP-completeness*; W. H. Freeman and Co.: New York, 1979.

(9) Ponzano, G.; Regge, T.; Semiclassical Limit of Racah coefficients. In *Spectroscopic and Group Theoretical Methods in Physics*; Bloch, F., Ed.; North-Holland: Amsterdam, 1968; p 1.

(10) Schulten, K.; Gordon, R. G. *J. Math. Phys.* **1975**, *16*, 1961, 1971.

(11) Askey, R. *Orthogonal Polynomials and Special Functions*; SIAM: Philadelphia, PA, 1975. Koekoek, R.; Swarttouw, R. F. *The Askey-Scheme of Hypergeometric Orthogonal Polynomials and its q-Analogue*; Technische Universiteit Delft: Delft, Netherlands, 1998.

(12) Anderson, R. W.; Aquilanti, V.; da S. Ferreira, C. *J. Chem. Phys.* **2008**, *129*, 161101.

(13) Aquilanti, V.; Haggard, H. M.; Littlejohn, R. G.; Poppe, S.; Yu, L. Asymptotics of the Wigner 6j-symbol in a 4j-model. Preprint, 2009.

(14) Neville, D. *J. Math. Phys.* **1971**, *12*, 2438.

(15) Ragni, M.; Bitencourt, A. P. C.; da S. Ferreira, C.; Aquilanti, V.; Anderson, R. W.; Littlejohn, R. G. *Int. J. Quantum Chem.*, DOI: 10.1002/qua.22117.

(16) Nikiforov, A. F.; Suslov, S. K.; Uvarov, V. B. *Classical Orthogonal Polyomials of a Discrete Variable*; Springer-Verlag: Berlin, 1991.

(17) Bruschi, M.; Calogero, F.; Droghei, R. *Adv. Math. Phys.* **2009**, 268134.

(18) Arvesu, J.; Coussement, J.; Van Assche, W. *J. Comp. Appl. Math.* **2003**, *153*, 19.

(19) Gross, J. L.; Tucker, T. W. *Topological Graph Theory*; Dover: New York, 1987.

(20) Fack, V.; Lievens, S.; Van der Jeugt, J. *Discr. Math.* **2002**, *245*, 1. Van Dyck, D.; Brinkmann, G.; Fack, V.; McKay, B. D. *Comput. Phys. Commun.* **2005**, *173*, 61.

(21) Kramer, P.; Lorente, M. *J. Phys. A: Math. Gen* **2002**, *35*, 8563.

(22) At the end of section 2.1 the embedding of 9*j* (I) into the orientable, genus-1 torus *T* was considered. The fact that $K_{3,3}$ has the same nonorientable and orientable genus is exceptional: most graphs have different values for *g* and *c*.

(23) Aquilanti, V.; Bitencourt, A. C. P.; da S, Ferreira, C.; Marzuoli, A.; Ragni, M. *Phys. Scr.* **2008**, *78*, 058103.

(24) Aquilanti, V.; Bitencourt, A. C. P.; da S. Ferreira, C.; Marzuoli, A.; Ragni, M. *Theor. Chem. Acc.* **2009**, *123*, 237.

(25) Carfora, M.; Marzuoli, A.; Rasetti. M. Quantum Tetrahedra. *J. Phys. Chem. A*, submitted for publication.

(26) Penrose, R. Angular Momentum: an approach to combinatorial space-time, in: Bastin, T. (Ed.), *Quantum Theory and Beyond*; Cambridge University Press: Cambridge, U.K., 1971; p 151.

(27) Aquilanti, V.; Haggard, H. M.; Littlejohn, R. G.; Yu, L. *J. Phys. A: Math. Theor.* **2007**, *40*, 5637.

(28) Aquilanti, V.; Caligiana, A. *Chem. Phys. Lett.* **2002**, *366*, 157. Avery, J.; Avery, J. *Generalized Sturmians and Atomic Spectra*; World Scientific: Singapore, 2006.

(29) Watson, J. K. G. *J. Phys. A: Math. Gen.* **1999**, *32*, 6901.

(30) Bailey, D. H. At http://crd.lbl.gov/dhbailey/mpdist/, 2006.

(31) Amit, D. J.; Roginsky, D. V. I. *J. Phys. A: Math. Gen.* **1979**, *12*, 689.

(32) Littlejohn, R. G.; Yu, L. Uniform semiclassical approximation of the Wigner 6j symbol in terms of rotation matrices. *J. Phys. Chem. A*, submitted for publication.

JP905212A